Ultrafast Charge-carrier Dynamics of Copper Oxide Nanocrystals

Brandon Born[1,*], Jeffrey D. A. Krupa[1], Simon Geoffroy-Gagnon[1], Ilija R. Hristovski[1], Christopher M. Collier[2], and Jonathan F. Holzman[1,*]

[1]School of Engineering, The University of British Columbia, Okanagan campus, Kelowna, B.C. V1V 1V7, Canada.

[2]School of Engineering, The University of Guelph, 50 Stone Road East, Guelph, Ontario, N1G 2W1, Canada.

Keywords: semiconductor nanocrystals, ultrafast charge-carrier dynamics, transient absorption pump-probe spectroscopy, femtosecond carrier-carrier scattering, trap-assisted recombination, mid-gap state, exciton-exciton annihilation

ABSTRACT: In this work, a detailed investigation is carried out on copper oxide, in the form of cupric oxide (CuO) nanocrystals. Particular attention is paid to the bandstructure and ultrafast charge-carrier dynamics. Transient absorption spectroscopy is carried out with an above-bandgap pump beam and below-bandgap probe beam to glean insight on the relaxation and recombination dynamics of the CuO nanocrystals at various pump fluences. Three time constants are apparent. The first time constant varies with pump fluence from 330 fs to 630 fs, and it is attributed to momentum relaxation via carrier-carrier scattering in the valence band as well as exciton-exciton annihilation. The second time constant is constant at 2 ps, and it is attributed to energy relaxation via carrier-phonon scattering within the valence band. The third time constant is constant at 50 ps, and it is attributed to trapping and recombination, due to the high density of trap states within the CuO nanocrystals. Such findings lay the foundation for future studies and applications of the emerging CuO material system.

Cupric oxide (CuO), or tenorite, is a semiconductor of rapidly growing interest. The interest in CuO has emerged within applied physics—largely from its potential for use in photovoltaics. Its absorption characteristics span the visible spectrum,[1-2] and its formation of copper vacancies and oxygen interstitials supports its use as a p-type lattice.[3] It has recently been shown that p-type copper oxide thin-films can be integrated with n-type metal oxide thin-films to form cost-effective photovoltaic p-n heterojunctions.[4-6] At the same time, CuO has recently been shown to exhibit ultrafast relaxation and recombination dynamics, which can support its use in all-optical switching.[7] However, an adequate understanding of its optical absorption characteristics and subsequent ultrafast charge-carrier dynamics has proven to be challenging.

A major challenge to the understanding of CuO is the nanocrystalline morphology that the material typically forms. The differing nanocrystal sizes and phases of the nanocrystalline morphology have led to disparities for the optical absorption characteristics of the CuO nanocrystals—with reports of an indirect bandgap of approximately 1.2 eV[8,9] and/or a direct bandgap ranging from 1.3 to 3.0 eV.[8,10-17] The nanocrystalline morphology also leads to complexities in the evolution of the ultrafast charge-carrier dynamics within the CuO nanocrystals, due largely to mid-gap trap states within the bandgap created by the nanocrystals' large surface area. Therefore, an accurate understanding of the fundamental charge-carrier trapping and relaxation dynamics in CuO nanocrystals is essential to future applications of CuO nanocrystals.

The work of Othonos *et al.* has been a major step to gain an understanding of the absorption and ultrafast charge-carrier dynamics of CuO nanowires.[3] The authors applied transient absorption spectroscopy to investigate CuO nanowires with diameters of 200 nm and lengths of 10 μm. It was proposed that the absorption and ultrafast charge-carrier dynamics are defined largely by the photoexcitation of electrons into the conduction band (CB) and the resulting relaxation of a transient population of holes within the valence band (VB).

In this work, the absorption and ultrafast charge-carrier dynamics of CuO nanocrystals are explored further. Optical absorption spectroscopy is applied to the CuO nanocrystals to define the bandstructure, revealing a bandgap of 1.55 eV. Transient absorption spectroscopy is then applied to the CuO nanocrystals, with varying pump fluence levels, to characterize the ultrafast charge-carrier dynamics. The theoretical models and experimental findings reveal that the charge-carriers are subject to femtosecond-duration momentum relaxation (via carrier-carrier scattering) within the VB, followed by picosecond-duration energy relaxation (via carrier-phonon interaction). The subsequent band-edge and trap-assisted recombination (via mid-gap states) shows indications of exciton-exciton annihilation. These findings can lay the groundwork for future applications of this material.

The CuO nanocrystals in this study are fabricated using a similar technique to that used by Johan *et al.*[12] Glass slides are cleaned using isopropyl and deionized water, dried with clean dry air, and sputtered with copper to form thin films. High temperature annealing is then applied at 600°C for two hours in ambient air to create the CuO phase—as opposed to the Cu_2O (cuprous oxide) phase that is formed at temperatures lower than 300°C.[12,18] The annealing process described here produced the best structural uniformity and spectral absorption characteristics, for CuO film thicknesses ranging from 20 nm to 200 nm. Films with sufficient quality could not be formed with thicknesses below 20 nm.

It is found that the CuO nanocrystal size is a function of the CuO film thickness. Figure 1 shows the trend for CuO film thicknesses of 20, 60, 100, and 200 nm, which yield CuO nanocrystal sizes (i.e., diameters) of roughly 50, 130, 140, and 300 nm, respectively. The corresponding scanning electron microscopy (SEM) images are shown in the figure insets. The CuO films with a nanocrystal diameter of 50 nm and a thickness of 20 nm are selected for further investigation in the remainder of

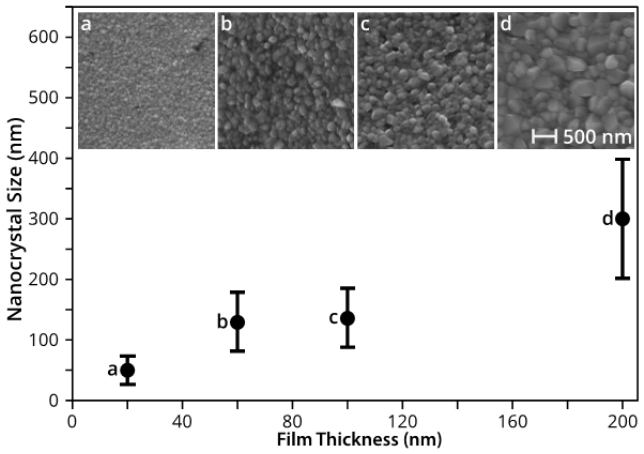

Figure 1. The CuO nanocrystal size as a function of the film thickness. The films have thicknesses of (a) 20, (b) 60, (c) 100, and (d) 200 nm, with nanocrystal sizes of 50, 130, 140, and 300 nm, respectively. The insets show SEM images of the nanocrystals.

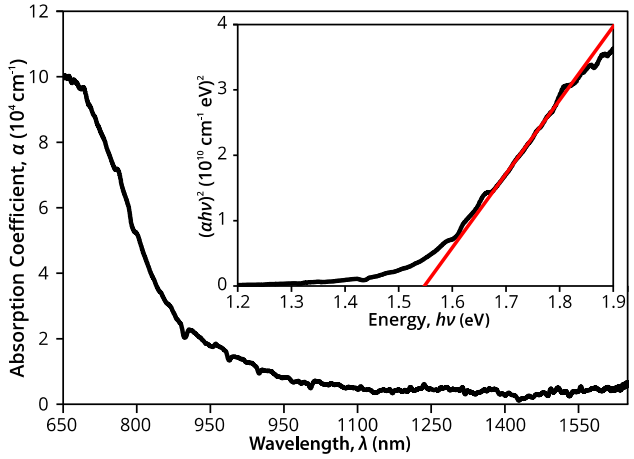

Figure 2. Optical absorption characteristics for the CuO nanocrystals. The absorption coefficient, α, is shown as a function of the wavelength, λ. A Tauc plot is shown in the inset, as $(\alpha h\nu)^2$ versus energy, $h\nu$, in black, with a linear fit shown in red. From this Tauc plot, the direct bandgap of the CuO nanocrystals is defined to be $E_g = 1.55$ eV.

this study. They are sufficiently small to yield a strong dependence on trap states, and are near the border of the regime for weak exciton confinement, which is approximately three times the Bohr exciton radius, a_0.[19] Here, the Bohr exciton radius is estimated to be $a_0 = \varepsilon_r \varepsilon_0 h^2/\pi\mu e^2 \approx 6 \pm 4$ nm, where h is Planck's constant, e is the electronic charge, ε_0 is the permittivity of free space, ε_r is the dielectric constant,[11,20] and the reduced mass, μ, ranges significantly in the literature.[11,13,21] (The Bohr exciton radius has previously been reported to range from 6.6 to 28.7 nm.)[22]

The optical absorption characteristics of the CuO nanocrystals are shown in Figure 2. The absorption coefficient, α, is displayed as a function of the wavelength, λ, which is calculated from the percent power absorbed, given by $1 - e^{-\alpha d}$, where d is the film thickness. The power absorbed is measured via transmission-reflection measurements[23] with a Yokogawa AQ6370 optical spectrum analyzer. The results show finite absorption across the displayed spectrum, which is attributed to a high density of trap states between the VB and CB of the nanocrystalline CuO material.[7] A Tauc plot, shown in the inset, is used to extract the bandgap, E_g, via the direct bandgap relation, $(\alpha h\nu)^2 = B^2(h\nu - E_g)$, where B is an arbitrary constant, ν is the photon frequency, and $h\nu$ is the photon energy.[23] An extrapolation of the linear region from 1.67 eV to 1.80 eV of the Tauc plot down to the horizontal axis identifies the bandgap to be $E_g = 1.55 \pm 0.05$ eV. The error here is quantified through repeated measurements with different samples and spectral sources. This measured bandgap is within the range seen in the literature for CuO.[12-17] There is also a notable Urbach tail, extending out to lower energies, which is characteristic of optical absorption via defect states in disordered semiconductor media.[24] The authors note that the bandgap for CuO nanocrystals will, in general, depend on the nanocrystal size. Decreasing the nanocrystal size increases the density of trap states, which encroach into the bandgap from the band edges. This is seen as a red-shift on E_g.[25] However, the bandgap will begin to increase when the nanocrystal size approaches the Bohr exciton radius due to quantum confinement. This is seen as a blue-shift on E_g.[25] Rehman *et al.* tested CuO nanocrystals with radii of 11–29 nm and observed these effects.[26] The nanocrystals for our study, having a radius of 25 nm, fall in this range and likely see a blue-shift from the calculated bulk crystal's bandgap of 1.25 eV.[27]

The charge-carrier dynamics that evolve within the CuO nanocrystals are revealed by way of transient absorption spectroscopy.[28-29] The collinear free-space pump and probe laser pulses are generated by an erbium-doped fibre laser (Toptica FFS-SYS-2B), emitting at a wavelength of 1550 nm for the probe beam, with a synchronized second harmonic stage emitting at a wavelength of 780 nm for the pump beam. The pulses have a 100 fs duration and 90 MHz repetition rate and are focused using a 40× microscope objective onto the CuO nanocrystals. Translation from across the sample, perpendicular to the optical axis, shows negligible changes to the results, indicating the nanocrystals are highly uniform. Translation parallel to the optical axis, out of the focal plane, is well controlled via nano-actuators (Newport, 8302), to ensure that reproducible beam fluences are applied. As the CuO nanocrystals have a bandgap of $E_g = 1.55$ eV, the experiment uses an above-bandgap pump photon energy of $E_{pump} = 1.6$ eV, at a wavelength of 780 nm, and a below-bandgap probe photon energy of $E_{probe} = 0.8$ eV, at a wavelength of 1550 nm. The selected photon energies, being $E_{pump} > E_g$ and $E_{probe} < E_g$, are

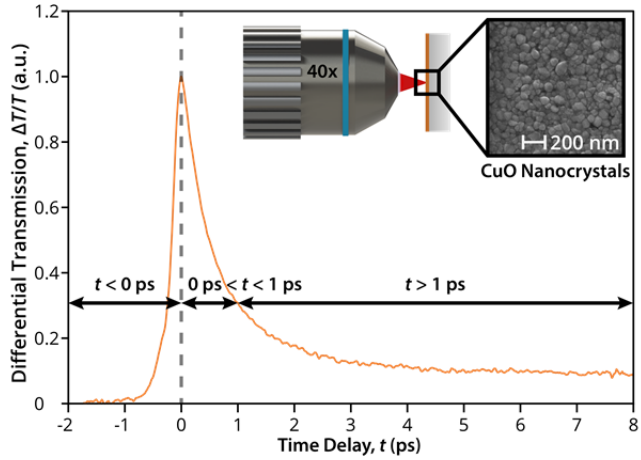

Figure 3. Transient absorption characteristics for the CuO nanocrystals. The pump and probe beams are focused onto the layer of nanocrystals using a 40× microscope objective, as seen in the inset. The transmitted probe beam power is measured as a function of the pump-probe time delay. The results, displayed as normalized differential transmission of the probe beam, $\Delta T/T$, are divided into four intervals: prior to zero time delay, $t < 0$ ps; at zero time delay, $t = 0$ ps; within the first picosecond after zero time delay, 0 ps $< t <$ 1 ps; after the first picosecond, $t > 1$ ps.

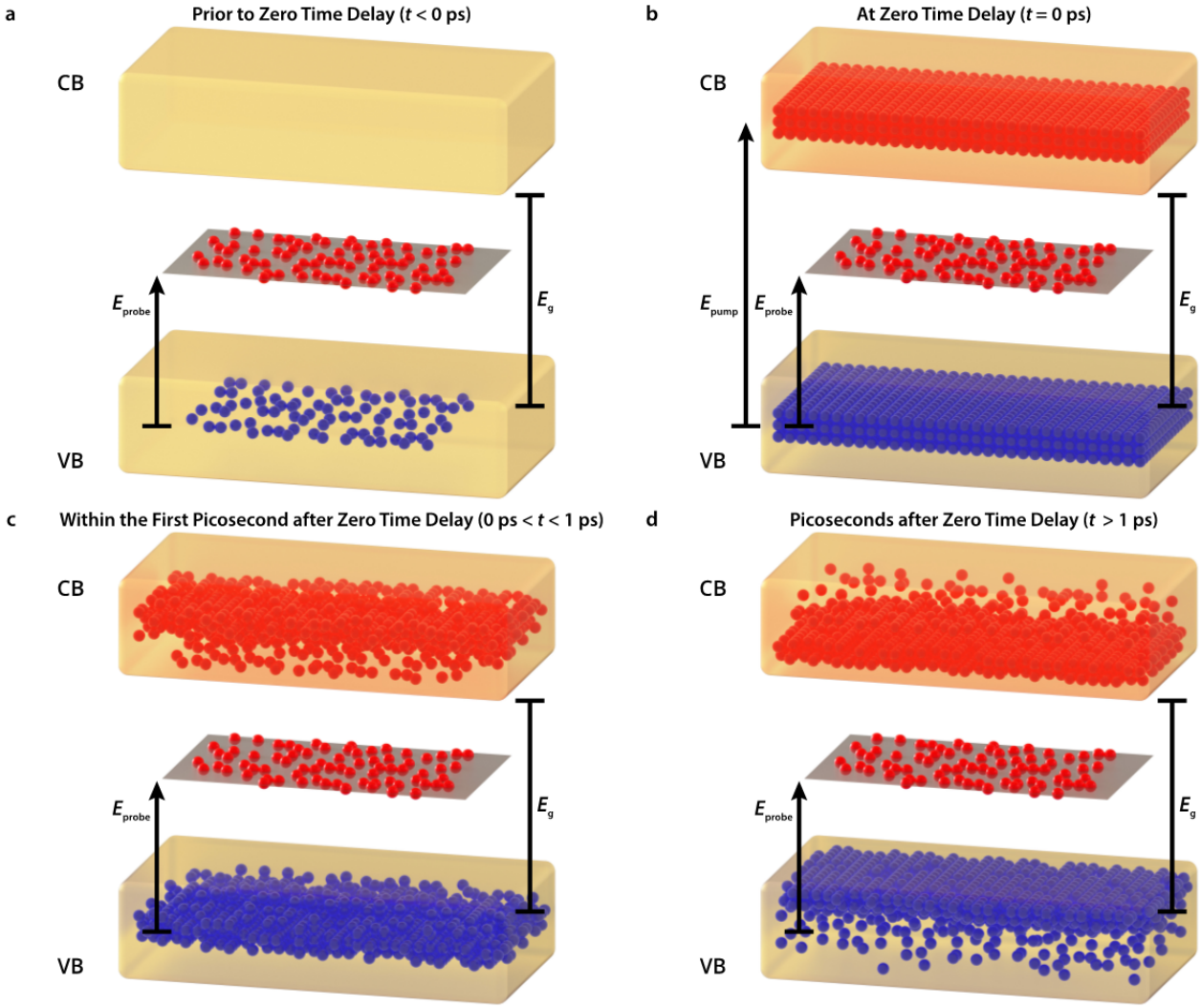

Figure 4. Illustration of the charge-carrier dynamics in the bandstructure of CuO nanocrystals having a bandgap of $E_g = 1.55$ eV. Photogenerated holes (blue) and electrons (red) are shown in the bandstructure at four time intervals: (a) prior to zero time delay, $t < 0$ ps, the VB and CB are populated by photogenerated holes and electrons from the probe beam, which has a photon energy of $E_{\text{probe}} = 0.8$ eV; (b) at zero time delay, $t = 0$ ps, additional holes and electrons are photogenerated by the pump beam, which has an energy of $E_{\text{pump}} = 1.6$ eV; (c) within the first picosecond after zero time delay, 0 ps $< t < 1$ ps, the photogenerated holes in the VB undergo momentum relaxation due to carrier-carrier scattering; and (d) after the first picosecond, $t > 1$ ps, the photogenerated holes in the VB undergo energy relaxation and trap-assisted recombination.

key for the study of this p-type material. The high pump photon energy allows it to photoexcite electrons from the VB to the CB. The low probe photon energy allows it to remain sensitive to charge-carrier dynamics evolving within the VB, as the probe beam will be predominately subject to absorption from the top of the VB to midgap states. Midgap states are known to play a major role in semiconductor nanocrystal films[30] (and are needed to explain the results that unfold in the following analyses). Representative experimental results are shown in Figure 3 as normalized differential transmission, $\Delta T/T$, of the probe beam as a function of the time delay, t, between the pump and probe pulses. The time delay axis has been divided into four segments. The interval prior to zero time delay is defined by $t < 0$ ps. The point of time at zero time delay is defined by $t = 0$ ps. The interval within the first picosecond after zero time delay is defined by 0 ps $< t < 1$ ps. The interval following the first picosecond is defined by $t > 1$ ps.

The evolution of the charge-carrier dynamics in the bandstructure of the CuO nanocrystals is illustrated in Figure 4. Prior to zero time delay, $t < 0$ ps, the bandstructure is populated by electrons (red) and holes (blue) in the manner depicted by Figure 4(a). Given the low photon energy of the probe beam, $E_{\text{probe}} \approx E_g/2$, the probe beam predominantly photoexcites electrons from near the top of the VB to mid-gap states in the bandgap. (Such a proposition is similar to the proposed dynamics within CuS nanocrystals.)[31] The process is labelled in the figure by E_{probe}. Precisely at zero time delay, $t = 0$ ps, the CuO bandstructure is populated by charge-carriers in the manner depicted by Figure 4(b). The system here is subject to the aforementioned probe beam absorption as well as the newly-introduced pump beam absorption. Given the large energy of the pump beam, $E_{\text{pump}} > E_g$, the pump beam photoexcites a high density of electrons into the CB and holes in the VB, as labelled by E_{pump}. Initially, the photogenerated holes in the VB have a narrow distribution, which is seen as a large decrease to the probe beam's absorption from state-filling-induced bleaching, i.e., a large increase is seen in the probe beam's transmission due to the pump-induced increase of holes within the VB. Within the first picosecond after zero time delay, 0 ps $< t < 1$ ps, charge-carriers in the VB undergo momentum relaxation on a femtosecond

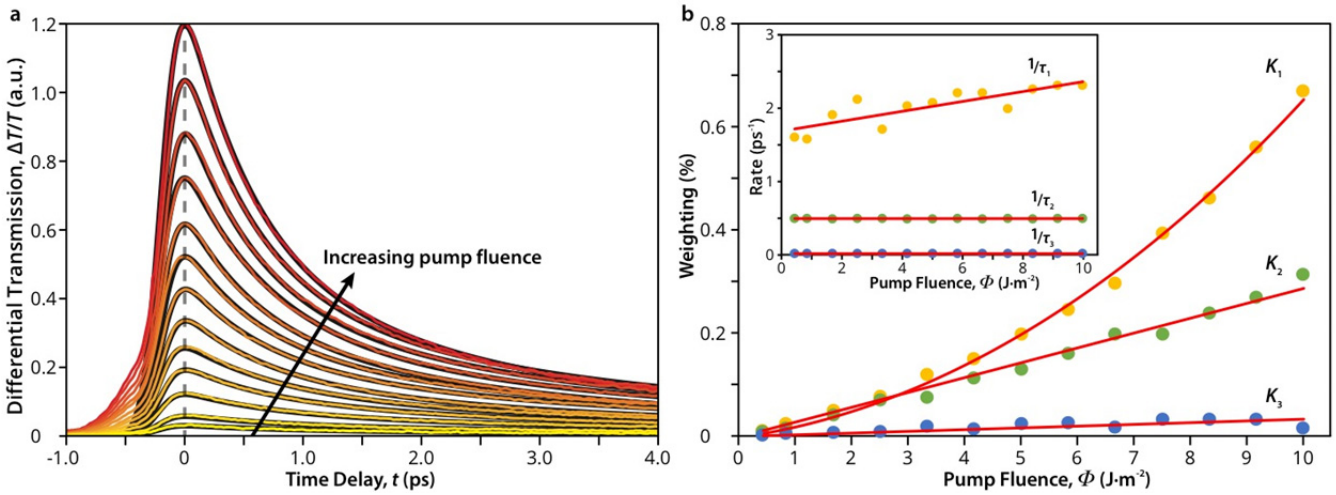

Figure 5. Time-resolved absorption characteristics for the 50 nm CuO nanocrystals. In (a), the experimental results for the normalized differential transmission, $\Delta T/T$, of the CuO nanocrystals are given for pump fluence increasing linearly from 0.4 J·m^{-2} (yellow) to 10 J·m^{-2} (red). Superimposed behind each experimental curve is the tri-exponential decay curve-fit (black). In (b), the weighting of the first time constant's term (top), K_1, the weighting of the second time constant's term (middle), K_2, and the weighting of the third time constant's term (bottom), K_3, are plotted as a function of the pump fluence, Φ. The inset shows the rates of the first (top), $1/\tau_1$, second (middle), $1/\tau_2$, and third (bottom), $1/\tau_3$, time-constants as a function of Φ. Trendlines are shown in red.

timescale, as depicted by Figure 4(c). The distribution of charge-carriers broadens due to carrier-carrier scattering, which rapidly decreases the number of holes that occupy the VB states undergoing probe beam absorption. This is seen as a rapid decrease in the probe beam's transmission. In the following picoseconds, for $t > 1$ ps, the holes in the VB undergo energy relaxation on a picosecond timescale and relax upwards towards the VB edge due to carrier-phonon interactions, as depicted by Figure 4(d). This further decreases the probe beam's transmission. Once the holes reach the VB edge, trap-assisted electron-hole recombination takes place to return the system to equilibrium.

The proposed charge-carrier dynamics are explored further to substantiate the interpretations of momentum relaxation (via carrier-carrier scattering), energy relaxation (via carrier-phonon interaction), and recombination (via midgap states). Given that rates at which charge-carriers undergo relaxation can vary with the photogenerated charge-carrier density, N,[32-34] the transient absorption analyses are repeated with varying pump fluences to witness variations in the rates (if any). The experimental results are shown in Figure 5.

Figure 5(a) shows the differential transmission of the probe beam, $\Delta T/T$, for 13 different pump fluences, increasing linearly from 0.4 J·m^{-2} to 10 J·m^{-2}. The $\Delta T/T$ recovery follows a tri-exponential decay that is dependent on pump fluence and independent of probe fluence. (Approximately 13% of the pump fluence is absorbed by the 20 nm thick nanocrystal film, based on the results of Figure 2.) Curve-fitting is applied via a tri-exponential function, $\Delta T/T(t) = K_1 e^{-t/\tau_1} + K_2 e^{-t/\tau_2} + K_3 e^{-t/\tau_3}$, where τ_1, τ_2, and τ_3 are time constants, and K_1, K_2, and K_3 are weightings (i.e., amplitudes). The curve-fitting parameters are extracted by convolving the tri-exponential function with the autocorrelation of the pump and probe pulses and employing iterative least-squares minimization. The curve-fitting shows strong agreement to the experimental results, with an average R-squared value of 0.999. The fitted curves are shown superimposed (in black) on the experimental results.

The three processes that exhibit the observed tri-exponential decay are characterized in Figure 5(b). This figure shows the rates for the time constants, $1/\tau_1$, $1/\tau_2$, and $1/\tau_3$, and the weightings, K_1, K_2, and K_3, as a function of the pump fluence, Φ. Trendlines are shown in red. The dependencies of the rates and weightings on Φ give insight into the underlying charge-carrier dynamics.

The first time constant, τ_1, is characterized for increasing pump fluence by a weighting, K_1, that has nearly linear growth (albeit with a small superlinear component) and a rate, $1/\tau_1$, that is nearly constant (albeit with a small linear component). We first consider the more standard linear response of K_1 and constant response of $1/\tau_1$. The responses are indicative of momentum relaxation, which in this case involves carrier-carrier scattering in the VB. The first time constant τ_1 varies from 330 fs to 630 fs, over the range of pump fluences. Such values are comparable to those seen for carrier-carrier scattering and momentum relaxation in other materials.[28] Moreover, these observations and interpretations agree with those proposed by Othonos *et al.* for CuO nanowires, for which a time constant of 400 fs was seen at lower fluence levels with a 770 nm probe beam.[3] (However, our 1550 nm probe beam, with a photon energy of only 0.8 eV, suggests that the state-filling-induced bleaching experienced by our probe beam is for transitions between VB and mid-gap states.) We next consider the more unusual superlinear response of K_1 and linear response of $1/\tau_1$—the beginnings of which were hinted at in the work of Othonos *et al.*[3] A similar initial rapid decay has been seen in other semiconductor nanocrystals, with a superlinear trend in the amplitude (and an increasing rate) with respect to pump fluence. The semiconductor nanocrystals include ZnCdS,[35] ZnO,[36] TiO_2,[37] CdS,[38] CdSe,[39] and Cu_xS.[40] This superlinear dependence is an indicator of exciton-exciton annihilation, which emerges following the saturation of trap states at sufficiently high pump fluence.[41-42] Trap state saturation leads to the preferential populating of charge-carriers at band edges, where they experience rapid recombination via exciton-exciton annihilation.[25,38-40,43] The superlinear growth in amplitude of our first process can be explained by this trap state saturation and emergence of exciton-exciton annihilation. At the same time, the linear trend in $1/\tau_1$, with respect to pump fluence, is supported by the higher-order kinetics of exciton-exciton annihilation. In general, highly photoexcited semiconductor nanocrystals exhibit second-order kinetics via two-body (exciton-exciton) Auger recombination and third-order kinetics via three-body (electron-electron-hole or electron-hole-hole) Auger recombination.[44] The rate of two-body Auger recombination is proportional to N,[39] and the rate of three-body Auger recombination is proportional to N^2.[45] Thus, our observed linearity between $1/\tau_1$ and N (and thus the pump fluence) suggests that there is a strong contribution of

exciton-exciton annihilation in this first process. (It is worth noting that CuO is known to establish highly-correlated charge-carriers, as seen by its formation of excitons with large binding energies and remarkably long lifetimes,[46] and exciton-exciton annihilation has been reported in the literature for Cu_2O.)[47]

The second time constant, τ_2, is constant at 2 ps over the range of pump fluences, and it is associated with energy relaxation involving carrier-phonon scattering in the VB and scattering to trap states. The value for τ_2 is comparable to those seen for energy relaxation in other materials[28,48] and is in agreement with that seen for energy relaxation by Othonos *et al.*[3] Moreover, the rate of energy relaxation, corresponding to the $1/\tau_2$ curve in the inset of Figure 5(b), is constant with respect to Φ, which indicates that the carrier-phonon scattering is independent of Φ and thus N as well.[34] The associated weighting of the second time constant's term, denoted by K_2, as a function of Φ, is seen in Figure 5(b). The linear trend seen here is indicative of standard state-filling-induced bleaching, which is proportional to N.[50]

The third time constant, τ_3, is constant at 50 ps over the range of pump fluences, and it is associated with trapping and recombination of charge-carriers. The long duration of this process matches typical time constants seen for trap-assisted charge-carrier recombination in semiconductor nanocrystals.[41,49,51] The authors note that the associated weighting of the third time constant's term, denoted by K_3, is positive, which indicates that the observed response is dominated by state-filling-induced bleaching of transitions from the VB up to mid-gap states. This is in contrast to free-carrier absorption, which would induce a negative change in transmission. (We do not see a transition from positive to negative probe transmission for any of our conditions, like those seen by Othonos *et al.* for a few of their probe energies, and this allows us to rule out secondary photoexcitation of electrons from mid-gap states or the conduction band up to higher states in the conduction band.)[3] Ultimately, the weighting K_3 is linearly proportional to Φ, as seen in the inset of Figure 5(b), and this is further evidence that the probe is subject to absorption between states at the edge of the VB and mid-gap states.

Given the importance of trap states in this third time constant, a free-carrier dynamical model is applied to characterize surface recombination in the CuO nanocrystals. It is assumed that the nanocrystals are uniformly illuminated to form an initial photogenerated charge-carrier density of N_0. The charge-carriers then undergo diffusion and recombination in accordance with

$$\frac{\partial N(r,\theta,t)}{\partial t} = N_0\delta(t) + D\nabla^2 N(r,\theta,t) - \frac{N(r,\theta,t)}{\tau_\mathrm{b}}, \qquad (1)$$

where free-carrier photoexcitation is approximated by the delta function, $\delta(t)$, diffusion along the radial dimension, r, is defined by the diffusion coefficient, D, and bulk recombination is defined by the bulk recombination lifetime, τ_b. The diffusing free-carriers ultimately reach the outer radius, at $r = a$, and undergo surface recombination in accordance with the boundary condition $-D\partial N(r=a,\theta,t)/\partial r = S_\mathrm{v} N(r=a,\theta,t)$, where the surface recombination velocity is S_v. This model can be greatly simplified by assuming that the system has no dependence on the polar angle, θ, and by assuming that the nanocrystal's radius is much less than the diffusion length, i.e., the diffusion coefficient is sufficiently large to ensure that $D \gg S_\mathrm{v} a$. With these simplifications, the solution for the charge-carrier density becomes $N(t) \approx N_0 e^{-t/\tau_3}$, where the recombination rate is $1/\tau_3 \approx 1/\tau_\mathrm{b} + S_\mathrm{v} R$ and $R = 3/a$ is the surface-to-volume ratio of the spherical nanocrystal.[7] Given the small radius of the nanocrystals, $a =$ 25 nm, and the measured recombination lifetime of $\tau_3 =$ 50 ps, the surface recombination velocity is estimated to be $S_\mathrm{v} \approx 2\times10^4$ m·s^{-1}. To the authors' best knowledge, a value for the surface recombination velocity of CuO has not been reported in literature, but the value reported here is comparable to those seen for CdS[49] and InP.[52] It is worth noting that a comparison to this work's other (larger) nanocrystals shows that the time constant τ_3 increases as the radius increases, as one expects for trap-assisted charge-carrier recombination, while the other two time constants, τ_1 and τ_2, exhibit minimal change as the radius increases, as one expects for their association to momentum and energy relaxation.

Within this work, a detailed investigation was carried out on the bandstructure and ultrafast charge-carrier dynamics of CuO nanocrystals. The bandgap was measured to be 1.55 ± 0.05 eV. This aligns with recent experimental studies, finding a direct bandgap[12-17] at 1.4–1.8 eV, and emerging theoretical studies,[17,21] going beyond Standard Density Functional Theory to show a direct bandgap at 1.25 eV for bulk CuO.[27] Both theoretically and experimentally, there appears to be a higher direct transition[17,26-27,53] near 3.0 eV, which may be the cause for the disparity in absorption characteristics. Transient absorption spectroscopy was carried out with an above-bandgap pump photon energy of 1.6 eV and a below-bandgap probe photon energy of 0.8 eV. The differential transmission of the probe beam through the CuO nanocrystals was measured for various pump fluences, and three time constants were apparent in the recovery. The first time constant, ranging from 330 fs to 630 fs, had a rate that scaled linearly with pump fluence and a weighting that scaled superlinearly with the pump fluence. The underlying mechanisms for this first time constant were attributed to momentum relaxation via carrier-carrier scattering within the VB and (what the authors believed to be) the first observation of exciton-exciton annihilation in CuO. The second time constant was constant at 2 ps, with a weighting that scaled linearly with the pump fluence, and its underlying mechanism was attributed to energy relaxation via carrier-phonon scattering within the VB. The third time constant was constant at 50 ps, with a weighting that scales linearly with the pump fluence, and its underlying mechanism was attributed to trapping and recombination, due to the high density of trap states within the bandstructure. It is hoped that the knowledge of the bandstructure and charge-carrier dynamics put forward in this work can lay the foundation for future studies and applications of the CuO material system.

AUTHOR INFORMATION

Corresponding Authors
*E-mail (B. Born): brandon.born@ubc.ca
*E-mail (J. F. Holzman): jonathan.holzman@ubc.ca

Notes
The authors declare no competing financial interest.

ACKNOWLEDGMENT

This study is supported by the Natural Sciences and Engineering Research Council of Canada (341487-12), Canadian Foundation for Innovation (LOF 16659), and Western Economic Diversification. We thank the Charles E. Fipke Foundation for use of the STAR SEMLab at the University of British Columbia's Okanagan Campus.

REFERENCES

1. Bu, I. Y. Y.; Novel All Solution Processed Heterojunction using P-type Cupric Oxide and N-type Zinc Oxide Nanowires for Solar Cell Applications, *Ceram. Int.* **2013,** *39*, 8073–8078.
2. Moskvin, A. S.; Loshkareva, N. N.; Sukhorukov, Y. P.; Sidorov, M. A.; Samokhvalov, A. A.; Characteristic Features of the Electronic Structure of Copper Oxide (CuO): Initiation of the Polar Configuration Phase and Middle-IR Optical Absorption, *J. Exp. Theor. Phys.* **1994,** *78*, 967–993.

3. Othonos, A.; Zervos, M.; Ultrafast Hole Carrier Relaxation Dynamics in P-type CuO Nanowires, *Nanoscale Res. Lett.* **2011,** *6*, 622–626.
4. Wang, P.; Zhao, X.; Li, B.; ZnO-coated CuO Nanowire Arrays: Fabrications, Optoelectronic Properties, and Photovoltaic Applications, *Opt. Express* **2011,** *19*, 11271–11279.
5. Sanal, K. C.; Vikas, L. S.; Jayaraj, M. K.; Room Temperature Deposited Transparent P-channel CuO Thin Film Transistors, *Appl. Surf. Sci.* **2014,** *297*, 153–157.
6. Kidowaki, H.; Oku, T.; Akiyama, T.; Suzuki, A.; Jeyadevan, B.; Cuya, J.; Fabrication and Characterization of CuO-based Solar Cells, *J. Mater. Sci. Res.* **2012,** *1*, 138–143.
7. Born, B.; Geoffroy-Gagnon, S.; Krupa, J. D. A.; Hristovski, I. R.; Collier, C. M.; Holzman, J. F.; Ultrafast All-Optical Switching via Subdiffractional Photonic Nanojets and Select Semiconductor Nanoparticles, *ASC Photonics* **2016,** *3*, 1095–1101.
8. Dimopoulos, T.; Peić, A.; Müllner, P.; Neuschitzer, M.; Resel, R.; Abermann, S.; Postl, M.; List, E. J. W.; Yakunin, S.; Heiss, W.; Brückl, H.; Photovoltaic Properties of Thin Film Heterojunctions with Cupric Oxide Absorber, *J. Renewable Sustainable Energy* **2013,** *5*, 011205-1–011205-11.
9. Rakhshani, A. E.; Barakat, F. K.; Optical constants of reactively sputtered cupric oxide films, *Mater. Lett.* **1987,** *6*, 37–40.
10. Pierson, J. F.; Thobor-Kech, A.; Billard, A.; Cuprite, paramelaconite and tenorite films deposited by reactive magnetron sputtering, *Appl. Surf. Sci.* **2003,** *210*, 359–367.
11. Ching, W. Y.; Xu, Y.-N.; Wong, K. W.; Ground-state and optical properties of Cu_2O and CuO crystals, *Phys. Rev. B* **1987,** *40*, 7684–7695.
12. Johan, M. R.; Suan, M. S. M.; Hawari, N. L.; Ching, H. A.; Annealing effects on the properties of copper oxide thin films prepared by chemical deposition, *Int. J. Electrochem. Sci.* **2011,** *6*, 6094–6104.
13. Zhang, Q.; CuO nanostructures: Synthesis, characterization, growth mechanisms, fundamental properties, and applications, *Prog. Mater. Sci.* **2014,** *60*, 208–337.
14. Meyer, B. K. et al. Binary Copper Oxide Semiconductors: From Materials Towards Devices, *Phys. Status Solidi B* **2012,** *249*, 1487–1509.
15. Parhizkar, M.; Singh, S.; Nayak, P. K.; Kumar, N.; Muthe, K. P.; Gupta, S. K.; Major, S. S.; Nanocrystalline CuO Films Prepared by Pyrolysis of Cu-Arachidate LB Multilayers, *Colloid Surf. A* **2005,** *257*, 277–282.
16. Patil, V.; Jundale, D.; Pawar, S.; Chougule, M.; Godse, P.; Patil, S.; Raut B.; Shashwati S.; Nanocrystalline CuO Thin Films for H_2S Monitoring: Microstructural and Optoelectronic Characterization, *J. Sens. Technol.* **2011,** *1*, 36–46.
17. Gattinoni, C.; Michaelides, A.; Atomistic details of oxide surfaces and surface oxidation: the example of copper and its oxides, *Surf. Sci. Rep.* **2015,** *70*, 424–447.
18. Khojier, K.; Savaloni, H.; Sadeghi, Z.; A comparative investigation on growth, nanostructure and electrical properties of copper oxide thin films as a function of annealing conditions, *J. Theor. Appl. Phys.* **2014,** *8*, 116-1–116-8.
19. Ekimov, A. J.; Hachre, F.; Schanne-Klein, M. C.; Richard, D.; Flytzanis, C.; Kudryavtsev, I. A.; Yazeva, T. V.; Rodina, A. V.; Efros, A. L. J.; Absorption and intensity-dependent photoluminescence measurements on CdSe quantum dots: assignment of the first electronic transitions, *Opt. Soc. Am. B* **1993,** *10*, 100–107.
20. West, C. J.; Hull, C.; *International Critical Tables of Numerical Data, Physics, Chemistry and Technology,* E. Washburn, McGraw-Hill, New York, 2003, 6, 76.
21. Wu, D.; Zhang Q.; LSDA+U study of cupric oxide: Electronic structure and native point defects, *Phys. Rev. B* **2006,** *73*, 235206-1–235206-6.
22. Borgohain, K.; Mahamuni, S.; Formation of single-phase CuO quantum particles, *J. Mater. Res.* **2002,** *17*, 1220–1223.
23. Ganjoo, A.; Golovchak, R.; Computer program PARAV for calculating optical constants of thin films and bulk materials: case study of amorphous semiconductors, *J. Optoelectron. Adv. Mater.* **2008,** *10*, 1328–1332.
24. Dhineshbabu, N. R.; Rajendran, V.; Nithyavathy, N.; and Vetumperumal R.; Study of structural and optical properties of cupric oxide nanoparticles, *Appl. Nanosci.* **2015,** *6*, 933–939.
25. Wheeler, D. A.; Zhang, J. Z.; Exciton dynamics in semiconductor nanocrystals, *Adv. Mat.* **2013,** *25*, 2878–2896.
26. Rehman, S.; Mumtaz, A.; Hasanain, S. K.; Size effects on the magnetic and optical properties of CuO nanoparticles, *J. Nanopart. Res.* **2011,** *13*, 2497–2507.
27. Ekuma, C. E.; Anisimov, V. I.; Moreno, J.; Jarrell, M.; Electronic structure and spectra of CuO, *Eur. Phys. J. B* **2014,** *87*, 1–6.
28. Othonos, A.; Probing ultrafast carrier and phonon dynamics in semiconductors, *J. Appl. Phys.* **1998,** *83*, 1789–1830.
29. Born, B.; Krupa, J. D. A.; Geoffroy-Gagnon, S.; Holzman, J. F.; Integration of photonic nanojets and semiconductor nanoparticles for enhanced all-optical switching, *Nat. Comm.* **2015,** *6*, 8097-1–8097-9.
30. Nagpal, P.; Klimov, V. I.; Role of mid-gap states in charge transport and photoconductivity in semiconductor nanocrystal films, *Nat. Comm*. **2011,** *2*, 486–1–486-7.
31. Brelle, M. C.; Torres-Martinez, C. L.; McNulty, J. C.; Mehra, R. K.; Zhang, J. Z.; Synthesis and characterization of Cu_xS nanoparticles. Nature of the infrared band and charge-carrier dynamics, *Pure Appl. Chem.* **2000,** *72*, 101–117.
32. Young, J. F.; Kelly, P. J.; Henry, N. L.; Dharma-wardana, M. W. C.; Carrier density dependence of hot-electron scattering rates in quasi-equilibrium electron-hole plasmas, *Solid State Comm.* **1991,** *78*, 343–346.
33. Hendry, E.; Koeberg, M.; Pijpers, J.; Bonn, M.; Reduction of carrier mobility in semiconductors caused by charge-charge interactions, *Phys. Rev. B* **2007,** *75*, 233202-1–233202-4.
34. Tang, C. L.; Erskine, D. J.; Femtosecond Relaxation of Photoexcited Nonequilibrium Carriers in $Al_xGa_{1-x}As$, *Phys. Rev. Lett.* **1983,** *51*, 840–843.
35. Ernsting, N. P.; Kaschke, M.; Weller, H.; Katsikas, L.; Colloidal $Zn_{1-x}Cd_xS$: Optical saturation of the exciton band and primary photochemistry studied by subpicosecond laser flash photolysis, *J. Opt. Soc. Am. B* **1990,** *7*, 1630–1637.
36. Cavaleri, J. J.; Skinner, D. E.; Colombo, D. P.; Bowman, R. M.; Femtosecond study of the size-dependent charge carrier dynamics in ZnO nanocluster solutions, *J. Chem. Phys.* **1995,** *103*, 5378–5386.
37. Philip Colombo, D.; Roussel, K. A.; Saeh, J.; Skinner, D. E.; Cavaleri, J. J.; Bowman, R. M.; Femtosecond study of the intensity dependence of electron-hole dynamics in TiO_2 nanoclusters, *Chem. Phys. Lett.* **1995,** *232*, 207–214.
38. Zhang, J. Z.; Ultrafast studies of electron dynamics in semiconductor and metal colloidal nanoparticles: effects of size and surface, *Acc. Chem. Res.* **1997,** *30*, 423–429.
39. Roberti, T. W.; Cherepy, N. J.; Zhang, J. Z.; Nature of the power-dependent ultrafast relaxation process of photoexcited charge carriers in II-VI semiconductor quantum dots: Effects of particle size, surface, and electronic structure, *J. Chem. Phys.* **1998,** *108*, 2143–2151.

40. Zhang, J. Z.; Interfacial charge carrier dynamics of colloidal semiconductor nanoparticles, *J. Phys. Chem. B* **2000,** *104*, 7239–7253.
41. Zhang, J. Z.; Wang, Z.-J.; Liu, J.; Chen, S.; Liu, G.-Y.; *Self-Assembled Nanostructures,* D. J. Lockwood, Springer, New York, 2003, 226–255.
42. Wheeler, D. A.; Huang, J. A.; Newhouse, R. J.; Zhang, W. F.; Lee, S. T.; Zhang, J. Z.; Ultrafast exciton dynamics in silicon nanowires, *J. Phys. Chem. Lett.* **2012,** *3*, 766–771.
43. Sun, D.; Rao, Y.; Reider, G. A.; Chen, G.; You, Y.; Brézin, L.; Harutyunyan, A. R.; Heinz, T. F.; Observation of rapid exciton-exciton annihilation in monolayer molybdenum disulfide, *Nano Lett.* **2014,** *14*, 5625–5629.
44. Huang, L.; Krauss, T. D.; Quantized bimolecular auger recombination of excitons in single-walled carbon nanotubes, *Phys. Rev. Lett.* **2006,** *96*, 057407-1–057407-4.
45. Klimov, V. I.; Mikhailovsky, A. A.; McBranch, D. W.; Leatherdale, C. A.; Bawendi, M. G.; Quantization of multiparticle auger rates in semiconductor quantum dots, *Science* **2000,** *287*, 1011–1013.
46. Kazimierczuk, T.; Fröhlich, D.; Scheel, S.; Stolz, H.; Bayer, M.; Giant Rydberg Excitons in the Copper Oxide Cu2O, *Nature* **2014,** *514*, 343–347.
47. Jang, J. I.; Wolfe, J. P.; Auger recombination and biexcitons in Cu_2O: A case for dark excitonic matter, *Phys. Rev. B* **2006,** *74*, 045211-1–045211-16.
48. Othonos, A.; Lioudakis, E.; Philipose, U.; Ruda, H. E.; Ultrafast carrier dynamics in band edge and broad deep defect emission ZnSe nanowires, *Appl. Phys. Lett.,* **2007,** *91*, 241113-1–241113-3.
49. Jurienas, S.; Stepankevieius, V.; Strumskis, M.; Zukauskas, A.; Carrier recombination in CdS nanocrystals under single-electron and high-density excitation, *Semicond. Sci. Technol.* **1995,** *10*, 302–309.
50. Klimov, V. I.; Spectral and dynamical properties of multiexcitons in semiconductor nanocrystals, *Annu. Rev. Phys. Chem.* **2007,** *58*, 635–673.
51. Yong, C. K.; Joyce, H. J.; Lloyd-Hughes, J.; Gao, Q.; Tan, H. H.; Jagadish, C.; Johnston, M. B.; Herz, L. M.; Ultrafast Dynamics of Exciton Formation in Semiconductor Nanowires, *Small* **2012,** *8*, 1725–1731.
52. Holzman, J. F.; Strasser, P.; Wüest, R.; Robin, F.; Erni, D.; Jäckel, H.; Ultrafast Carrier Dynamics in InP Photonic Crystals, *Nanotechnology* **2005,** *16*, 949–952.
53. Son, D. I.; You, C. H.; Kim, T. W.; Structural, optical, and electronic properties of colloidal CuO nanoparticles formed by using a colloid-thermal synthesis process, *Appl. Surf. Sci.* **2009,** *255*, 8794–8797.

FOR TABLE OF CONTENTS USE ONLY
Manuscript Title: Ultrafast Charge-carrier Dynamics of Copper Oxide Nanocrystals

Names of Authors: Brandon Born, Jeffrey D. A. Krupa, Simon Geoffroy-Gagnon, Ilija R. Hristovski, Christopher M. Collier, and Jonathan F. Holzman

Table of Contents Graphic: